MODELING BSM EFFECTS ON THE HIGGS TRANSVERSE-MOMENTUM SPECTRUM IN AN EFT APPROACH*

Agnieszka Ilnicka

Physics Institute, University of Zürich
Winterthurerstrasse 190, 8057 Zürich, Switzerland
and
Physics Department, ETH Zürich
Otto-Stern-Weg 5, 8093 Zürich, Switzerland
and
Paul Scherrer Institute, 5232 Villigen PSI, Switzerland
ailnicka@physik.uzh.ch

(Received January 22, 2018)

After the discovery of the Higgs boson in 2012, LHC is currently studying its properties. The measurements of small deviations from the SM predictions can be the only way to access new physics, if no new resonances will be found. The bottom-up Effective Field Theory offers a consistent approach, with new higher dimension operators built of Standard Model fields (SMEFT). We discuss how this approach works in the case of the transverse momentum spectrum of the Higgs particle. In our calculation, we augmented the Standard Model with three additional dimension-six operators corresponding to modifications of the top and bottom Yukawa couplings, and a point-like Higgs coupling to gluons. We also discuss the inclusion of the chromomagnetic operator. We present and discuss the impact of these three operators on the p_{T} spectra at the NLL+NLO accuracy, and show how it can be approximately extended to the NNLL+NNLO level. We find that such modifications, while affecting the total rate within the current uncertainties, can lead to significant distortions in the spectrum shape.

DOI:10.5506/APhysPolBSupp.11.307

1. Introduction

In 2012, ATLAS and CMS observed the 125 GeV scalar resonance [1, 2] which could be identified as the Higgs boson of the Standard Model (SM). Despite the successes of the SM in describing the collider data, it fails in

* Presented at the Final HiggsTools Meeting, Durham, UK, September 11–15, 2017.

predicting well-established cosmological phenomena, *e.g.* the baryon asymmetry of the Universe or the existence of dark matter. For this reason, many beyond the SM (BSM) theories addressing these issues have been developed, which in particular often modify the Higgs boson properties. However, if new resonances exist beyond the reach of LHC, new physics will be manifested only in small deviations from the SM predictions. The topic of how to consistently account for these deviations, especially in the model-independent way, is still under discussion [3,4], but Effective Field Theory (EFT) proves to be a well-motivated approach. In the SMEFT bottom-up approach, the usual dimension-four operators of the SM are augmented by dimension-six operators[1], built of SM fields. With the use of experimental data, the values of the Wilson coefficients of these operators can then be fixed and via the top–down EFT translated into bound of parameters of a UV model of choice. For this, however, tools including dimension-six operators need to be developed and predictions made available. Since the Higgs p_{T} spectrum is an important observable, which will be measured at the LHC and will shed light on Higgs' properties, the aim is to develop a dedicated tool. In this proceeding, we report on the progress of the inclusion of relevant dimension-six operators which were implemented in the code for the calculation of the Higgs p_{T} spectra. It is based on the results presented in Refs. [7–10].

2. Transverse-momentum spectrum

Kinematical distributions provide an important handle on the determination of Higgs properties. One of the key observables is the Higgs transverse-momentum distribution, which was already measured in Run 1 [11–13], but will be measured with higher precision in Run 2 and the High Luminosity stage of the LHC[2]. The p_{T} spectrum provides more information than the total cross section, which is just one number, thus allowing to disentangle effects that remain hidden in the total rates. The fact that the Higgs is a scalar gives an additional simplification in modelling of p_{T} spectra using the narrow-width approximation, since the production and decay factorise.

The most abundant Higgs production channel at the LHC is gluon fusion, which, although being a loop-induced process, is highly enhanced by the dominance of the gluon density [15]. Therefore, we will limit ourselves to discuss only the spectra obtained in this channel. A significant amount of work has been dedicated to improve the precision of the predictions of the SM Higgs p_{T} spectrum. The first results at the lowest order ($\mathcal{O}(\alpha_{\mathrm{S}}^3)$) have been known for a long time [16,17]. It took nearly ten years until the $\mathcal{O}(\alpha_{\mathrm{S}}^4)$ corrections were computed [18–21] and another decade for the results at

[1] The full set of 59 dimension-six SMEFT operators has been presented in [5,6].
[2] The most recent results including 13 TeV data come from ATLAS [14].

the $\mathcal{O}(\alpha_S^5)$ accuracy [22–24]. The latter two were carried out in the heavy-top limit (HTL, *i.e.* $m_t^2 \gg M_H^2, p_{TH}^2$)[3]. The first partial results were also presented for the full massive case at NLO, however they are not completed yet [27].

The perturbative expansion is affected by large logarithmic terms of the form of $\alpha_S^n \ln^m(m_H^2/p_T^2)$, with $1 \leq m \leq 2n$ in the low-p_T region ($p_T \ll M_H$). This results in a singular behaviour of the distribution at p_T approaching zero. To cure this problem, a resummation of these terms to all orders in α_S [28] is needed. The resummation is carried out in impact parameter (b) space, and we follow the formalism of Ref. [29]. The resummed and fixed order results are then matched at intermediate p_T to avoid double counting

$$\left[\frac{d\sigma}{dp_T^2}\right]_{fo+ao} = \left[\frac{d\sigma}{dp_T^2}\right]_{fo} - \left[\frac{d\sigma^{(res)}}{dp_T^2}\right]_{fo} + \left[\frac{d\sigma^{(res)}}{dp_T^2}\right]_{ao}, \tag{1}$$

where "fo" corresponds to fixed order, and "ao" to all orders calculations. In the formalism of Ref. [29], a unitarity constraint is enforced, such that the integral of the p_T spectrum coincides with the corresponding total inclusive cross section computed at fixed order[4]. Top- and bottom-mass effects can be included in the resummed spectrum along the lines of Refs. [30, 31].

The inclusion of dimension-six and dimension-eight operators in the Higgs p_T spectrum has been considered in Refs. [32–36] and [37, 38], respectively. Most of the above studies, however, are limited to the high-p_T region of the spectrum and do not include small-p_T resummation.

3. Effective operators

The general form of SMEFT Lagrangian is

$$\mathcal{L} = \mathcal{L}_{SM} + \sum_i \frac{c_i}{\Lambda^2}\mathcal{O}_i\,, \tag{2}$$

where the SM is supplemented by the inclusion of a set of dimension-six operators[5] describing new physics effects at a scale Λ, which needs to be well above the electroweak scale. In our study, we consider the following four operators:

[3] Finite top-mass effects on the Higgs p_T distribution at $\mathcal{O}(\alpha_S^4)$ were estimated in Refs. [25, 26].

[4] By performing the resummation at next-to-leading logarithmic accuracy (NLL) and including the fixed order result up to $O(\alpha_S^3)$, we obtain NLO+NLL accuracy, and the integral of the spectrum is fixed to the NLO total cross section.

[5] Note that the only dimension-five operator corresponds to Majorana neutrino mass term and thus is uninteresting for the collider phenomenology.

$$\begin{aligned}\mathcal{O}_1 &= |H|^2 G^a_{\mu\nu} G^{a,\mu\nu}\,, & \mathcal{O}_2 &= |H|^2 \bar{Q}_{\rm L} H^c u_{\rm R} + \text{h.c.}\,,\\ \mathcal{O}_3 &= |H|^2 \bar{Q}_{\rm L} H d_{\rm R} + \text{h.c.}\,, & \mathcal{O}_4 &= \bar{Q}_{\rm L} H \sigma^{\mu\nu} T^a u_{\rm R} G^a_{\mu\nu} + \text{h.c.}\end{aligned} \tag{3}$$

These operators, in the case of single Higgs production, may be expanded as

$$\begin{aligned}\frac{c_1}{\Lambda^2}\,\mathcal{O}_1 &\to \frac{\alpha_{\rm S}}{\pi v} c_g h G^a_{\mu\nu} G^{a,\mu\nu}\,,\\ \frac{c_2}{\Lambda^2}\,\mathcal{O}_2 &\to \frac{m_t}{v} c_t h \bar{t}t\,,\\ \frac{c_3}{\Lambda^2}\,\mathcal{O}_3 &\to \frac{m_b}{v} c_b h \bar{b}b\,,\\ \frac{c_4}{\Lambda^2}\,\mathcal{O}_4 &\to c_{tg}\frac{g_S m_t}{2v^3}(v+h) G^a_{\mu\nu}(\bar{t}_{\rm L}\sigma^{\mu\nu} T^a t_{\rm R} + \text{h.c.})\,.\end{aligned} \tag{4}$$

The operator $\mathcal{O}_1$ corresponds to a contact interaction of the Higgs boson with gluons and has the same structure as the heavy-top limit (HTL) of the SM. The operators $\mathcal{O}_2$ and $\mathcal{O}_3$ describe modifications of the top and bottom Yukawa couplings respectively. The operator $\mathcal{O}_4$ is the chromomagnetic dipole-moment operator, which modifies the interactions between the gluons, top quark and Higgs boson[6] (here $\sigma^{\mu\nu} = \frac{i}{2}[\gamma^\mu, \gamma^\nu]$). In our convention, starting from the SILH basis [39,40], we express the Wilson coefficients as factors in the canonically normalised Lagrangian.

All the coefficients c_i can be probed in Higgs boson processes. In particular, c_t (and c_b) may be measured in the $t\bar{t}H$ (and $b\bar{b}H$) production modes. The coefficient c_b can also be accessed through the decay $H \to b\bar{b}$. The coefficient c_{tg}, instead, is constrained by top pair production [41]. The Higgs $p_{\rm T}$ spectrum measurement is the easiest approach to bound c_g. Note that the combined analysis of these measurements will allow to put stronger limits on the effective couplings.

4. Impact of the effective operators on the Higgs and Higgs+jet production

We now consider the contribution of the effective operators $\mathcal{O}_1, \mathcal{O}_2$ and $\mathcal{O}_4$ on the total production cross section, while omitting, for simplicity, the bottom contribution in $\mathcal{O}_3$. The relevant Feynman diagrams are shown in Fig. 1. The corresponding amplitude can be written as

$$\mathcal{M}\left(g(p_1) + g(p_2) \to H\right) = i\frac{\alpha_{\rm S}}{3\pi v}\epsilon_{1\mu}\epsilon_{2\nu}\left[p_1^\nu p_2^\mu - (p_1 p_2) g^{\mu\nu}\right] F(\tau)\,, \tag{5}$$

where $\tau = 4m_t^2/m_h^2$ and ϵ_1 and ϵ_2 are the polarization vectors of the incoming gluons. The contribution of the chromomagnetic operator to the function

[6] In this analysis, we do not consider the contribution of the chromomagnetic dipole operator of the bottom quark.

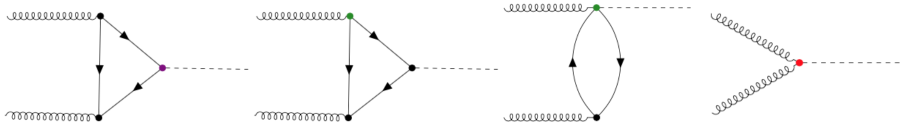

Fig. 1. (Colour on-line) Feynman diagrams contributing to $gg \to H$ production at LO. The possible insertions of dimension-six operators are marked in colour.

$F(\tau)$ has been addressed in the literature with contradicting results [42, 43] (see also Ref. [44]). In Ref. [42], it is found that the UV divergences in the bubble and triangle contributions cancel out. In the revised version of Ref. [43], it is instead stated that the UV divergence is present, and it has to be reabsorbed into the coefficient c_g.

Our results are consistent with the latter statement[7]. We find

$$F(\tau) = \Gamma(1+\epsilon)\left(\frac{4\pi\mu^2}{m_t^2}\right)^{\epsilon}\left(c_t F_1(\tau) + c_{g0} F_2(\tau) + \mathrm{Re}(c_{tg})\frac{m_t^2}{v^2} F_{30}(\tau)\right), \quad (6)$$

where

$$F_1(\tau) = \frac{3}{2}\tau\left[1 + (1-\tau) f(\tau)\right], \quad (7)$$

$$F_2(\tau) = 12, \quad (8)$$

$$F_{30}(\tau) = -\frac{6}{\epsilon} - 3\left[1 - \tau f(\tau) - 2g(\tau)\right], \quad (9)$$

with the functions $f(\tau)$ and $g(\tau)$ available *e.g.* in [7, 45]. The $1/\epsilon$ divergence can be reabsorbed in the $\overline{\mathrm{MS}}$ renormalization of the coefficient c_g

$$c_{g0} = c_g(\mu_\mathrm{R}) + \delta c_g \quad (10)$$

with

$$\delta c_g = \frac{m_t^2}{2v^2}\mathrm{Re}(c_{tg})\Gamma(1+\epsilon)(4\pi)^{\epsilon}\left(\frac{1}{\epsilon} + \ln\frac{\mu^2}{\mu_\mathrm{R}^2}\right), \quad (11)$$

where μ_R denotes the renormalization scale of c_g and μ the 't Hooft scale. The final result reads

$$F(\tau) = c_t F_1(\tau) + c_g(\mu_\mathrm{R}) F_2(\tau) + \mathrm{Re}(c_{tg})\frac{m_t^2}{v^2} F_3(\tau), \quad (12)$$

where

$$F_3(\tau) = -3\left(1 - \tau f(\tau) - 2g(\tau) + 2\ln\frac{\mu_\mathrm{R}^2}{m_t^2}\right). \quad (13)$$

[7] Note also the sign correction with respect to Ref. [7].

In the HTL $m_t^2 \gg m_h^2$, we have

$$F_1(\tau) \to 1\,, \qquad F_2(\tau) \to 12\,, \qquad F_3(\tau) \to 6\left(1 - \ln\frac{\mu_{\rm R}^2}{m_t^2}\right)\,. \tag{14}$$

In the SM, we have $c_t = 1$ and $c_g = c_{tg} = 0$, so that $F(\tau) \to F_1(\tau)$.

Based on bounds on c_{tg} presented in Ref. [41], we calculated that the impact on the total cross section is less than 20%. We conclude that, although smaller than the impact of c_g, the effect of c_{tg} can still be important, despite that the chromomagnetic operator provides a contribution which is formally $\mathcal{O}(\lambda_t^2)$ with respect to the others. In a strict expansion in $\alpha_{\rm S}$, it can be neglected. This is what we will do while presenting the spectra.

Unlike the c_t, c_b and c_g contributions which correspond to the rescaled SM and HTL of the SM results, the impact of the chromomagnetic operator needs a dedicated calculation of the corresponding amplitudes. In Fig. 2, the Feynman diagrams contributing to the gg-channel are presented, with marked diagrams which contribute also to the qg- and qq-channel when a fermion line replaces the two external gluon lines connected to the triple gluon vertex. In the case of gg-channel, the amplitude can be written in terms of external gluon polarisation vectors and the third rank tensor

$$\mathcal{A} = f_{abc}\mathcal{A}^{\mu\nu\rho}\epsilon_\mu(p_1)\epsilon_\nu(p_2)\epsilon_\rho(p_3)\,. \tag{15}$$

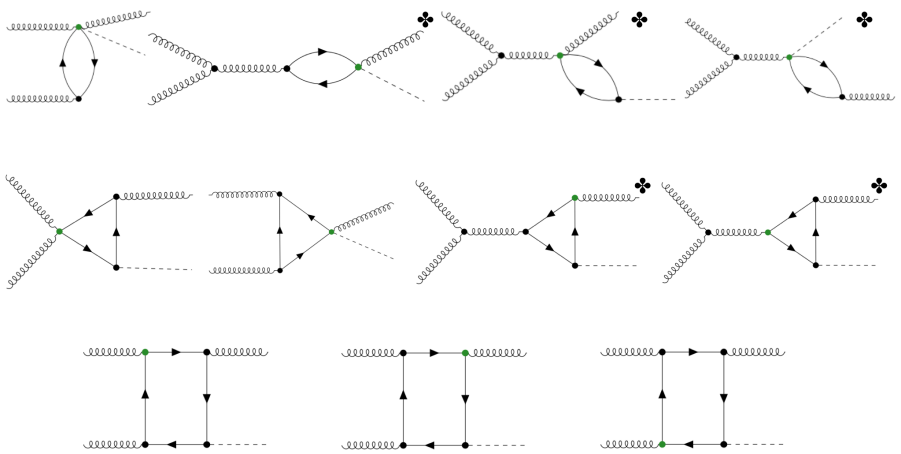

Fig. 2. (Colour on-line) Feynman diagrams contributing to $gg \to gH$ production with the inclusion of the chromomagnetic operator (marked in grey/green). Additionally the diagrams corresponding also to the qg- and qq-channel are marked in the upper corner.

The tensor can be expressed in terms of four form factors corresponding to the four tensor structures

$$\begin{aligned}\mathcal{A}^{\mu\nu\rho} &= F_1(p_1,p_2,p_3)\mathcal{Q}_1^{\mu\nu\rho} + F_2(p_1,p_2,p_3)\mathcal{Q}_2^{\mu\nu\rho} + F_3(p_1,p_2,p_3)\mathcal{Q}_3^{\mu\nu\rho} \\ &\quad + F_4(p_1,p_2,p_3)\mathcal{Q}_4^{\mu\nu\rho}\,. \end{aligned} \tag{16}$$

The form factors can be obtained by projecting the tensor amplitude applying the projectors combined from the $\mathcal{Q}_i$s. Then they require tensor reduction to be expressed in terms of the scalar loop integrals. The obtained form factors can then be redefined after squaring in the axial gauge for the external gluons, into ones which can be added in squares for the squared amplitude

$$|\mathcal{A}|^2 = |C_1|^2 + |C_2|^2 + |C_3|^2 + |C_4|^2\,. \tag{17}$$

Let us note here that only two form factors are independent and the other two can be obtained from the relations

$$\begin{aligned} C_3(s,t,u) &= -C_2(t,s,u)\,, \\ C_4(s,t,u) &= C_2(u,t,s)\,, \end{aligned} \tag{18}$$

where s,t,u are the usual Mandelstam variables. The details of calculations[8] and analytic results will be reported elsewhere [9, 10].

5. Calculational setup

In the next section, we present the p_{T} spectra of Higgs particle at NLL+NLO accuracy level, with the modifications coming from the effective operators. The calculation relies on the codes of Refs. [46, 47] and [30, 48]. The reference SM predictions are also shown in the figures, with the grey band on the lower panel showing the perturbative uncertainty. The uncertainties of the renormalization and factorization scales are estimated by performing the customary seven-point μ_{R}, μ_{F} variation, *i.e.* we consider independent variations within the range $\mu_0/2 \leq \mu_{\mathrm{F}}, \mu_{\mathrm{R}} \leq 2\mu_0$ with $1/2 < \mu_{\mathrm{R}}/\mu_{\mathrm{F}} < 2$, where $\mu_0 = \sqrt{p_{\mathrm{T}}^2 + m_H^2}/2$, and also the variation of the three resummation scales by a factor of two[9]. The values chosen for the effective coupling were guided by Eq. (14), *i.e.* to obtain the total cross section within 20% of the SM value, and currently available fits of the Wilson coefficients [49–51].

[8] We used the conventions of the Ref. [45].

[9] For the details of the calculation set up, see Ref. [7].

The above described calculations are the basis for the approximate extension to one order higher. To provide the approximate NNLL+NNLO SMEFT calculations, we used the NNLL+NNLO SM predictions, and then scaled them with the NLL+NLO calculations including the SMEFT operators

$$\left(\frac{\mathrm{d}\sigma}{\mathrm{d}p_{\mathrm{T}}}\right)^{\mathrm{SMEFT}}_{\mathrm{NNLL+NNLO}}(p_{\mathrm{T}}) = \frac{\left(\frac{\mathrm{d}\sigma}{\mathrm{d}p_{\mathrm{T}}}\right)^{\mathrm{SMEFT}}_{\mathrm{NLL+NLO}}(p_{\mathrm{T}})}{\left(\frac{\mathrm{d}\sigma}{\mathrm{d}p_{\mathrm{T}}}\right)^{\mathrm{SM}}_{\mathrm{NLL+NLO}}(p_{\mathrm{T}})} \left(\frac{\mathrm{d}\sigma}{\mathrm{d}p_{\mathrm{T}}}\right)^{\mathrm{SM}}_{\mathrm{NNLL+NNLO}}(p_{\mathrm{T}})\,. \tag{19}$$

It is important to note here that the NNLL+NNLO results [19–21] are known only in the heavy-top limit, with just an approximate inclusion of finite top mass effects, thus the exact calculation is not possible yet. We used SM results obtained with the numerical code `HRes` [31, 52]. Again, to estimate the scale uncertainties, we performed the same scale variations as mentioned above.

6. Results

We start our analysis by considering the individual contribution of exactly one operator, as presented in Fig. 3. Firstly, let us note that the uncertainty of the SM result, which is displayed as the grey band in the lower panel of the plot, is of $\sim \pm 20\%$ at the peak, but $\sim +50\%\ -30\%$ at $p_{\mathrm{T}} = 400$ GeV and above. Looking at the low-p_{T} region (0 GeV$\leq p_{\mathrm{T}} \leq$ 400 GeV), we can directly deduce that modifications of the bottom Yukawa coupling through c_b dominantly affect the low-p_{T} shape of the distribution. In fact, at very low p_{T}, we find effects that can even exceed the uncertainty of the SM prediction. As expected, $c_b < 1$ ($c_b > 1$) softens (hardens) the spectrum in that region[10]. The point-like Higgs-gluon coupling c_g, on the other hand, modifies the p_{T} shape most notably at large transverse momenta (400 GeV$\leq p_{\mathrm{T}} \leq$ 800 GeV), see Fig. 3 (b), where a positive (negative) c_g value hardens (softens) the spectrum. As expected, modifications of the top Yukawa have almost exclusively the effect of a normalisation of the total cross section. The deviations from the SM prediction through the dimension-six operators are within the scale uncertainty, although the differences in shape give some additional sensitivity to distinguish such effects.

Let us compare the above with Fig. 6 (a) where, again, the individual contributions of the operators are presented. As reference, the NNLL+NNLO SM predictions are shown in the figure as solid black line, with the grey

[10] We point out, however, that this is true only when small deviations of c_b from its SM value $c_b = 1$ are considered. In this case, the dominant effect of c_b is on the top–bottom interference. When c_b is significantly different from unity, the squared bottom-loop contribution can change the picture, see *e.g.* [53].

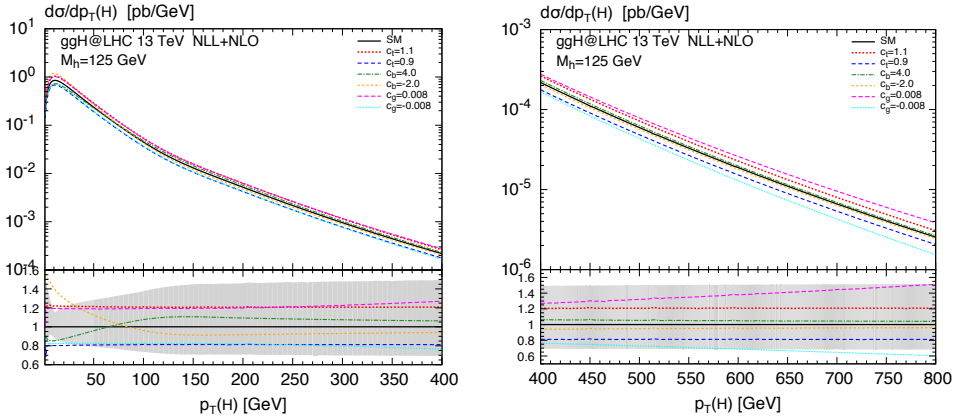

Fig. 3. Higgs transverse-momentum spectrum in the SM (black, solid) compared to separate variations of the dimension-six operators for (a) 0 GeV$\leq p_{\mathrm{T}} \leq$ 400 GeV and (b) 400 GeV$\leq p_{\mathrm{T}} \leq$ 800 GeV. The lower frame shows the ratio with respect to the SM prediction. The shaded band in the ratio indicates the uncertainty due to scale variations. The figures are taken from Ref. [7].

bands on the lower panel showing the perturbative uncertainties. The light grey band corresponds to the NLL+NLO uncertainty relative to the central scale NLL+NLO calculations, while the darker band corresponds to the NNLL+NNLO scale uncertainty relative to the NNLL+NNLO central scale calculation. This presentation allows us to observe the decrease of the uncertainty while going one order higher, by about a factor of two in the low- and intermediate-p_{T} range (up to around 250 GeV). In the higher p_{T} region, the uncertainties become more scattered due to statistical fluctuations. From the grey bands on the lower panel, it can be noticed that at the NLL+NLO accuracy all the curves are within the scale uncertainty, while in the NNLL+NNLO case, the effects of higher dimension operators exceed the uncertainties. This suggests that the accuracy of the calculations is a key ingredient when differentiating between different models and scenarios (see also [34]).

The simultaneous variation of more than a single coefficient, as considered in Figs. 4–5 and Fig. 6 (b), gives rise to more significant effects.

In Fig. 4, we present the simultaneous variation of c_t and c_g. Focusing on the impact of c_t and c_g, we note that the total cross section alone does not allow us to disentangle the effects of these two coefficients

$$\sigma \approx |12c_g + c_t|^2 \sigma_{\mathrm{SM}} \quad (\mathrm{HTL})\,. \tag{20}$$

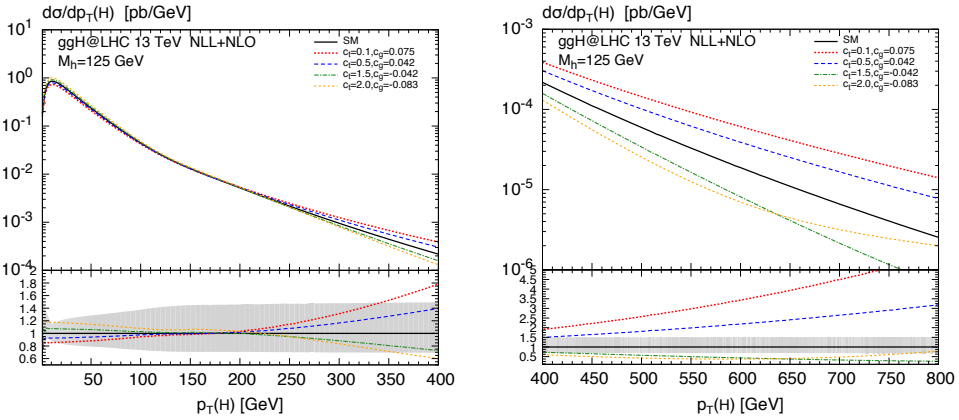

Fig. 4. (Colour on-line) Higgs transverse-momentum spectrum in the SM (black, solid) compared to simultaneous variations of c_t and c_g for (a) 0 GeV$\leq p_{\mathrm{T}} \leq$ 400 GeV and (b) 400 GeV$\leq p_{\mathrm{T}} \leq$ 800 GeV. The lower frame shows the ratio with respect to the SM prediction. The shaded band in the ratio indicates the uncertainty due to scale variations. The figures are taken from Ref. [7].

As already noted in the literature [33], the transverse momentum spectrum allows us to break this degeneracy. In this case, both the small- and high-p_{T} behaviour of the spectrum is altered by the different combinations of c_t and c_g coefficients. It is clear that in particular the large-p_{T} region offers a good discrimination between the different structures of Higgs-gluon interactions in terms of shape. Again, negative (positive) c_g values will soften (harden) the spectrum. The effects are well beyond the theoretical uncertainties already at NLL+NLO, especially in the high-p_{T} range (400–800 GeV). We note that the short-dashed yellow curve corresponding to $c_t = 2$, $c_g = -0.083$ develops a minimum in the ratio to the SM around $\sim$ 650 GeV. This is due to a compensation between the negative interference between the $\mathcal{O}_1$ and $\mathcal{O}_2$ operators, which is proportional to $c_g c_t$ and the contribution of $\mathcal{O}_1$ itself, which is proportional to c_g^2 and tends to produce a harder spectrum with respect to the SM prediction. The above behaviour, of dominance of subleading (dimension-eight) term, leads to question about the range of validity of EFT description.

Finally, we discuss spectra obtained by switching on all three SMEFT operators, as shown in Fig. 5 and Fig. 6. Our focus here is on scenarios with increased top-quark Yukawa coupling (up to $c_t = 1.5$). These scenarios would be of particular interest in the case in which the excess on the $t\bar{t}H$ rate over the SM prediction [54,55] should be confirmed. In order to compensate the increase in the cross section driven by $c_t > 1$, a negative c_g has been chosen. We observe a general tendency of the BSM spectra to fall below the

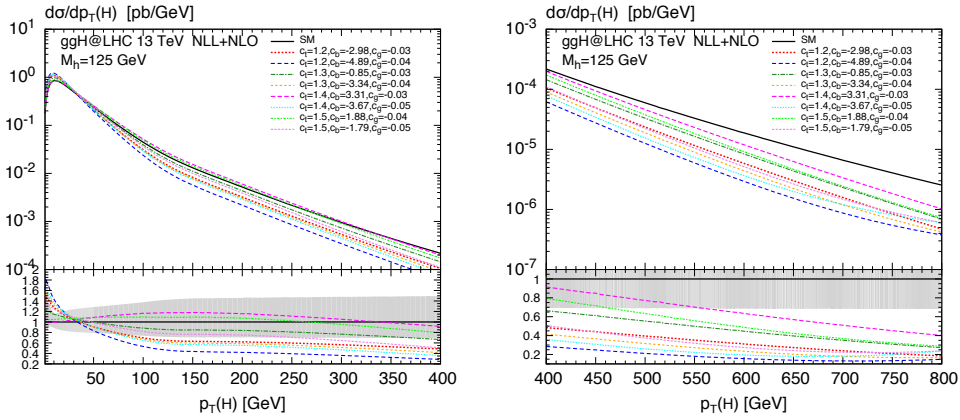

Fig. 5. Higgs transverse-momentum spectrum in the SM (black, solid) compared to simultaneous variations of c_t, c_g and c_b for (a) 0 GeV$\leq p_{\mathrm{T}} \leq$ 400 GeV and (b) 400 GeV$\leq p_{\mathrm{T}} \leq$ 800 GeV. The lower frame shows the ratio with respect to the SM prediction. The shaded band in the ratio indicates the uncertainty due to scale variations. The figures are taken from Ref. [7].

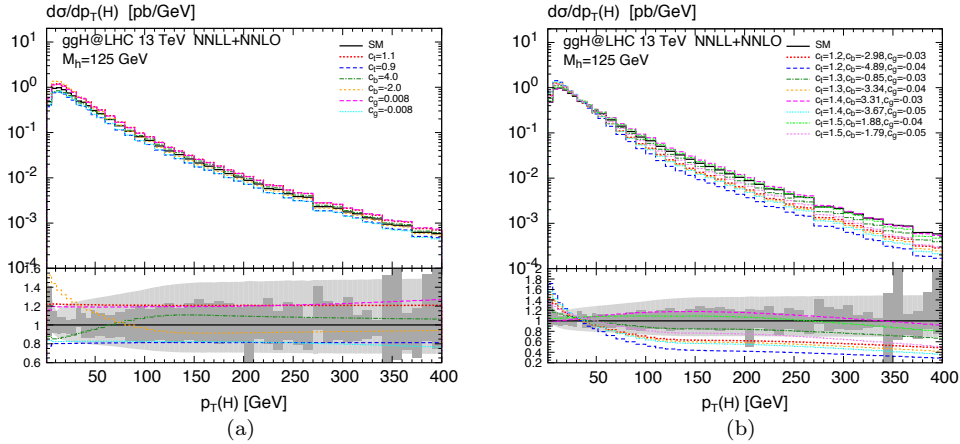

Fig. 6. Higgs transverse-momentum spectrum in the SM (black, solid) compared to (a) separate variations and (b) mixed contribution of the dimension-six operator for 0 GeV$\leq p_{\mathrm{T}} \leq$ 400 GeV. The lower frame shows the ratio with respect to the SM prediction. The shaded lighter and darker grey bands in the ratio indicate the uncertainty due to scale variations at NLL+NLO and NNLL+NNLO respectively. The figures are taken from Ref. [8].

SM prediction in the intermediate and high transverse-momentum range, which is due to the negative c_g contribution. The total rate is compensated by the enhancement in the low-p_{T} region, due to a combination of the nega-

tive c_g coefficient with both negative and positive c_b modifications. Overall, we find sizeable distortions of the p_{T} shapes due to the dimension-six operators far beyond the scale uncertainties of the NLL+NLO SM prediction. In Fig. 6 (b), we can observe that the further reduction of the scale uncertainty in the NNLL+NNLO case allows for a better discrimination between different scenarios.

We conclude this section with a comment on the validity of the EFT approach. The computation we have performed is carried out under the assumption that we can consider the effects of higher-dimensional operators as a "small" perturbation with respect to the SM result. This implies in particular that the effect of dimension-eight operators can be neglected. This is not obvious, given that we are studying also the large transverse-momentum region. To check the above assumption, we have repeated our calculations by dropping the $\mathcal{O}(1/\Lambda^4)$ suppressed terms originating from the square of the dimension-six contributions. We find that in most of the cases, the differences with respect to the results shown in Figs. 3–5 are very small, even at high transverse momenta. Only in the scenarios considered in Fig. 4 ($c_t = 0.1, c_g = 0.075$ and $c_t = 2, c_g = -0.083$), the $\mathcal{O}(1/\Lambda^4)$ effects are important, as the effects of subdominant terms become manifest, and thus, the corresponding quantitative results should be interpreted with care[11].

7. Conclusions

After the discovery of Higgs particle, one of the main challenges for the LHC is to collect data to enable precise comparison with the SM predictions. Especially if no new resonances will be found, these possible (small) deviations can point in the direction of new physics. For this purpose, the SMEFT framework may be used. In the SMEFT framework, BSM effects are parametrised through appropriate higher-dimensional operators in the model-independent way, and bounds on the corresponding Wilson coefficients can be set by comparing to the experimental data.

In this contribution, we have presented a computation of the transverse-momentum spectrum of the Higgs boson in which the SM prediction is supplemented by possible BSM effects. Such effects are modelled by augmenting the SM Lagrangian with appropriate dimension-six operators, related to the modifications of top and bottom Yukawa couplings and to the inclusion of a point-like ggH coupling. Our calculation consistently includes all the terms up to $\mathcal{O}(\alpha_{\mathrm{S}}^3)$ accuracy. Additionally, it is supplemented by soft-gluon resummation at NLL accuracy to obtain reliable predictions at small transverse momenta.

[11] More detailed discussion may be found in *e.g.* Refs. [4, 56].

We found that variations of different SMEFT operators manifest themselves in different regions of the Higgs p_{T} spectrum:

— a modification of the bottom-quark Yukawa coupling (c_b) induces effects almost exclusively at small transverse momenta,

— a point-like coupling of the Higgs boson to gluons (c_g) changes the shape of the distribution in the high-p_{T} tail,

— a change in the top-quark Yukawa coupling (c_t) contributes to the rescaling of the whole spectrum.

We can notice, from the presented spectra, that the shape of the transverse momentum distribution depends on the mass of the particle that mediates the Higgs-gluon coupling. The lower the mass of that particle, the softer is the resulting spectrum, and thus the enhancement of the bottom loop leads to the softest spectra, while the enhancement of the point-like coupling (corresponding to the infinite mass particle in the loop) to the hardest one.

We also have presented an approximate extension of the Higgs p_{T} spectra augmented with SMEFT operators to NNLL+NNLO level of accuracy. We started with state-of-the-art SM predictions and scale them by the relative SMEFT/SM effects at NLL+NLO (*i.e.* the ratios plotted in the lower panels of the figures). The NNLL+NNLO SM predictions are known only in the heavy-top limit, with just an approximate inclusion of top-mass effects, and thus the approach involving a scaling of the spectra was the only one possible. With the full top-mass-dependent results at NNLO, it would be desirable to redo the analysis in the same spirit as the one done in the NLL+NLO case.

Although in the spectra presented here, the contribution of the chromomagnetic operator was skipped, the calculation involving this operator is in progress and the corresponding results will be presented elsewhere [9, 10].

A.I. thanks M. Grazzini, M. Spira and M. Wiesemann for the collaboration on the presented work, and also additionally M. Grazzini and M. Spira for reading and corrections of the proceedings. This work is supported by the 7$^{\mathrm{th}}$ Framework Programme of the European Commission through the Initial Training Network HiggsTools PITN-GA-2012-316704.

REFERENCES

[1] G. Aad *et al.* [ATLAS Collaboration], *Phys. Lett. B* **716**, 1 (2013) `arXiv:1207.7214 [hep-ex]`].

[2] S. Chatrchyan *et al.* [CMS Collaboration], *Phys. Lett. B* **716**, 30 (2013) [`arXiv:1207.7235 [hep-ex]`].

[3] D. de Florian *et al.* [LHC Higgs Cross Section Working Group], *CERN Yellow Reports: Monographs* **2** (2017) DOI:10.23731/CYRM-2017-002 [arXiv:1610.07922 [hep-ph]].

[4] M. Boggia *et al.*, arXiv:1711.09875 [hep-ph].

[5] W. Buchmüller, D. Wyler, *Nucl. Phys. B* **268**, 621 (1986).

[6] B. Grzadkowski, M. Iskrzyński, M. Misiak, J. Rosiek, *J. High Energy Phys.* **1010**, 085 (2010) [arXiv:1008.4884 [hep-ph]].

[7] M. Grazzini, A. Ilnicka, M. Spira, M. Wiesemann, *J. High Energy Phys.* **1703**, 115 (2017) [arXiv:1612.00283 [hep-ph]].

[8] M. Grazzini, A. Ilnicka, M. Spira, M. Wiesemann, arXiv:1705.05143 [hep-ph].

[9] M. Grazzini, A. Ilnicka, M. Spira, in preparation, 2018.

[10] A. Ilnicka, Higgs Boson Production in Standard Model Effective Field Theory, University of Zurich, 2018.

[11] V. Khachatryan *et al.* [CMS Collaboration], *Eur. Phys. J. C* **76**, 13 (2016) [arXiv:1508.07819 [hep-ex]].

[12] V. Khachatryan *et al.* [CMS Collaboration], *J. High Energy Phys.* **1604**, 005 (2016) [arXiv:1512.08377 [hep-ex]].

[13] G. Aad *et al.* [ATLAS Collaboration], *Phys. Rev. Lett.* **115**, 091801 (2015) [arXiv:1504.05833 [hep-ex]].

[14] M. Aaboud *et al.* [ATLAS Collaboration], *J. High Energy Phys.* **1710**, 132 (2017) [arXiv:1708.02810 [hep-ex]].

[15] H.M. Georgi, S.L. Glashow, M.E. Machacek, D.V. Nanopoulos, *Phys. Rev. Lett.* **40**, 692 (1978).

[16] R.K. Ellis, I. Hinchliffe, M. Soldate, J.J. van der Bij, *Nucl. Phys. B* **297**, 221 (1988).

[17] U. Baur, E.W.N. Glover, *Nucl. Phys. B* **339**, 38 (1990).

[18] C.R. Schmidt, *Phys. Lett. B* **413**, 391 (1997).

[19] D. de Florian, M. Grazzini, Z. Kunszt, *Phys. Rev. Lett.* **82**, 5209 (1999) [arXiv:hep-ph/9902483].

[20] C.J. Glosser, C.R. Schmidt, *J. High Energy Phys.* **0212**, 016 (2002) [arXiv:hep-ph/0209248].

[21] V. Ravindran, J. Smith, W.L. Van Neerven, *Nucl. Phys. B* **634**, 247 (2002) [arXiv:hep-ph/0201114].

[22] R. Boughezal *et al.*, *J. High Energy Phys.* **1306**, 072 (2013) [arXiv:1302.6216 [hep-ph]].

[23] R. Boughezal *et al.*, *Phys. Rev. Lett.* **115**, 082003 (2015) [arXiv:1504.07922 [hep-ph]].

[24] X. Chen, T. Gehrmann, E.W.N. Glover, M. Jaquier, *Phys. Lett. B* **740**, 147 (2015) [arXiv:1408.5325 [hep-ph]].

[25] R.V. Harlander, T. Neumann, K. J. Ozeren, M. Wiesemann, *J. High Energy Phys.* **1208**, 139 (2012) [arXiv:1206.0157 [hep-ph]].

[26] T. Neumann, M. Wiesemann, *J. High Energy Phys.* **1411**, 150 (2014) [arXiv:1408.6836 [hep-ph].

[27] R. Bonciani *et al.*, *J. High Energy Phys.* **1612**, 096 (2016) [arXiv:1609.06685 [hep-ph]].

[28] J.C. Collins, D.E. Soper, G.F. Sterman, *Nucl. Phys. B* **261**, 104 (1985).

[29] G. Bozzi, S. Catani, D. de Florian, M. Grazzini, *Nucl. Phys. B* **737**, 73 (2006) [arXiv:hep-ph/0508068].

[30] H. Mantler, M. Wiesemann, *Eur. Phys. J. C* **73**, 2467 (2013) [arXiv:1210.8263 [hep-ph]].

[31] M. Grazzini, H. Sargsyan, *J. High Energy Phys.* **1309**, 129 (2013) [arXiv:1306.4581 [hep-ph]].

[32] C. Grojean, E. Salvioni, M. Schlaffer, A. Weiler, *J. High Energy Phys.* **1405**, 022 (2014) [arXiv:1312.3317 [hep-ph]].

[33] A. Azatov, A. Paul, *J. High Energy Phys.* **1401**, 014 (2014) [arXiv:1309.5273 [hep-ph]].

[34] U. Langenegger, M. Spira, I. Strebel, arXiv:1507.01373 [hep-ph]].

[35] F. Maltoni, E. Vryonidou, C. Zhang, *J. High Energy Phys.* **1610**, 123 (2016) [arXiv:1607.05330 [hep-ph]].

[36] N. Deutschmann, C. Duhr, F. Maltoni, E. Vryonidou, arXiv:1708.00460 [hep-ph]].

[37] R.V. Harlander, T. Neumann, *Phys. Rev. D* **88**, 074015 (2013) [arXiv:1308.2225 [hep-ph]].

[38] S. Dawson, I.M. Lewis, M. Zeng, *Phys. Rev. D* **90**, 093007 (2014) [arXiv:1409.6299 [hep-ph]].

[39] G.F. Giudice, C. Grojean, A. Pomarol, R. Rattazzi, *J. High Energy Phys.* **0706**, 045 (2007) [arXiv:hep-ph/0703164].

[40] R. Contino *et al.*, *J. High Energy Phys.* **1307**, 035 (2013) [arXiv:1303.3876 [hep-ph]].

[41] D. Buarque Franzosi, C. Zhang, *Phys. Rev. D* **91**, 114010 (2015) [arXiv:1503.08841 [hep-ph]].

[42] D. Choudhury, P. Saha, *J. High Energy Phys.* **1208**, 144 (2012) [arXiv:1201.4130 [hep-ph]].

[43] C. Degrande *et al.*, *J. High Energy Phys.* **1207**, 036 (2012) [*Erratum ibid.* **1303**, 032 (2013)] [arXiv:1205.1065 [hep-ph]].

[44] Y.T. Chien *et al.*, *J. High Energy Phys.* **1602**, 011 (2016) [arXiv:1510.00725 [hep-ph]].

[45] M. Spira, A. Djouadi, D. Graudenz, P.M. Zerwas, *Nucl. Phys. B* **453**, 17 (1995) [arXiv:hep-ph/9504378].

[46] G. Bozzi, S. Catani, D. de Florian, M. Grazzini, *Phys. Lett. B* **564**, 65 (2003) [arXiv:hep-ph/0302104].

[47] D. de Florian, G. Ferrera, M. Grazzini, D. Tommasini, *J. High Energy Phys.* **1111**, 064 (2011) [arXiv:1109.2109 [hep-ph]].

[48] R.V. Harlander, H. Mantler, M. Wiesemann, *J. High Energy Phys.* **1411**, 116 (2014) [arXiv:1409.0531 [hep-ph]].

[49] B. Dumont, S. Fichet, G. von Gersdorff, *J. High Energy Phys.* **1307**, 065 (2013) [arXiv:1304.3369 [hep-ph]].

[50] A. Falkowski, *Pramana* **87**, 39 (2016) [arXiv:1505.00046 [hep-ph]].

[51] A. Butter *et al.*, *J. High Energy Phys.* **1607**, 152 (2016) [arXiv:1604.03105 [hep-ph]].

[52] D. de Florian, G. Ferrera, M. Grazzini, D. Tommasini, *J. High Energy Phys.* **1206**, 132 (2012) [arXiv:1203.6321 [hep-ph]].

[53] U. Langenegger, M. Spira, A. Starodumov, P. Trueb, *J. High Energy Phys.* **0606**, 035 (2006) [arXiv:hep-ph/0604156].

[54] G. Aad *et al.* [ATLAS Collaboration], ATLAS-CONF-2016-080.

[55] S. Chatrchyan *et al.* [CMS Collaboration], CMS-PAS-HIG-16-022.

[56] A. Biekotter, J. Brehmer, T. Plehn, *Phys. Rev. D* **94**, 055032 (2016) [arXiv:1602.05202 [hep-ph]].